Measurement of the spin-transfer-torque vector in magnetic tunnel junctions

JACK C. SANKEY[1], YONG-TAO CUI[1], JONATHAN Z. SUN[2], JOHN C. SLONCZEWSKI[2]*, ROBERT A. BUHRMAN[1] AND DANIEL C. RALPH[1†]

[1]Cornell University, Ithaca, New York 14853, USA
[2]IBM T. J. Watson Research Center, Yorktown Heights, New York 10598, USA
*IBM RSM Emeritus
†e-mail: ralph@ccmr.cornell.edu

Published online: 25 November 2007; doi:10.1038/nphys783

The transfer of spin angular momentum from a spin-polarized current to a ferromagnet can generate sufficient torque to reorient the magnet's moment. This torque could enable the development of efficient electrically actuated magnetic memories and nanoscale microwave oscillators. Yet difficulties in making quantitative measurements of the spin-torque vector have hampered understanding. Here we present direct measurements of both the magnitude and direction of the spin torque in magnetic tunnel junctions, the type of device of primary interest for applications. At low bias V, the differential torque $\mathrm{d}\boldsymbol{\tau}/\mathrm{d}V$ lies in the plane defined by the electrode magnetizations, and its magnitude is in excellent agreement with recent predictions for near-perfect spin-polarized tunnelling. We find that the strength of the in-plane differential torque remains almost constant with increasing bias, despite a substantial decrease in the device magnetoresistance, and that with bias the torque vector also rotates out of the plane.

Magnetic tunnel junctions (MTJs) with MgO barriers can have extremely large magnetoresistance, and for this reason they are being pursued aggressively for applications in memory technologies and magnetic-field sensing[1–4]. Further, it has recently been demonstrated that the magnetic state of a nanoscale MTJ can be switched by a spin-polarized tunnel current via the so-called spin-transfer torque[5,6]. This is a promising new mechanism for the write operation of nanomagnetic memory elements[7] and for driving nanoscale microwave oscillators[8–10]. Although the presence of the spin torque has been unambiguously observed, its quantitative behaviour in an MTJ, especially its bias dependence, has yet to be understood in detail. One puzzling observation has been that, in comparison to the tunnel magnetoresistance, the differential spin torque has been found to depend very weakly on the junction bias[11]. Recent theoretical models attempt to quantify the spin torque's bias dependence in an MTJ, and to explain its relationship with the tunnel magnetoresistance[12–15]. To test these model calculations, a direct, quantitative measurement of how the spin torque varies with junction bias is highly desirable. Quantitative understanding of this bias dependence will also be important for the development and optimization of nanostructured MTJ spin-torque devices in memory applications.

Here we use the recently developed technique of spin-transfer-driven ferromagnetic resonance (ST-FMR)[16,17] to measure the bias and angular dependence of the spin-transfer torque $\boldsymbol{\tau}$ in MgO-based junctions. We demonstrate for the first time that ST-FMR can be used to achieve a quantitative understanding of spin torque in individual nanoscale devices. We define $\hat{\mathbf{m}}$ and $\hat{\mathbf{M}}_{\mathrm{fixed}}$ as unit vectors in the direction of the magnetic moments on the two sides of our magnetic tunnel junction and V as the bias voltage. Our measurements show that at low bias the in-plane component (in the direction $\hat{\mathbf{m}} \times (\hat{\mathbf{m}} \times \hat{\mathbf{M}}_{\mathrm{fixed}})$) of the spin transfer 'torkance' $\mathrm{d}\tau_{\parallel}/\mathrm{d}V$ on moment $\hat{\mathbf{m}}$ is equal, within the experimental accuracy ($\pm 15\%$), to the value predicted for an elastic tunnel current with a spin polarization $P = 0.66$ appropriate for our junctions[18]. We find $\mathrm{d}\tau_{\parallel}/\mathrm{d}V$ to be essentially bias independent, varying by less than 8% below 0.3 V, and seeming to increase slightly at even higher bias, where hot-electron effects may start to influence measurements. In contrast, the magnetoresistance decreases by 72% over our bias range. We also measure a perpendicular component $\mathrm{d}\tau_{\perp}/\mathrm{d}V$ (in the $\hat{\mathbf{m}} \times \hat{\mathbf{M}}_{\mathrm{fixed}}$ direction) that is non-zero only when $V \neq 0$, with a bias dependence corresponding to $\tau_{\perp}(V) \propto A_0 + A_1 V^2$ near $V = 0$ (with A_0 and A_1 constants). Our measurements can be interpreted within a simple model.

We have studied eight exchange-biased tunnel junctions with the layers (in nm) 5Ta/20Cu/3Ta/20Cu/15PtMn/2.5$Co_{70}Fe_{30}$/0.85Ru/3$Co_{60}Fe_{20}B_{20}$/1.25MgO/2.5$Co_{60}Fe_{20}B_{20}$/5Ta/7Ru deposited on an oxidized silicon wafer by the process described in ref. 19 (see Fig. 1a). The top magnetic layer (with moment direction $\hat{\mathbf{m}}$) is etched to a rounded rectangular cross-section with the long axis parallel to the exchange bias from the PtMn layer (the $\hat{y}$ direction), with size either $50 \times 100\,\mathrm{nm}^2$ or $50 \times 150\,\mathrm{nm}^2$. The bottom layer (moment direction $\hat{\mathbf{M}}_{\mathrm{fixed}}$) is left extended on the scale of tens of micrometres. All data in this paper are from one $50 \times 100\,\mathrm{nm}^2$ device; the other samples gave similar behaviour. Contact pads are originally fabricated in a four-point configuration, but we cut the top electrode close to the sample (Fig. 1b, left inset) before ST-FMR measurements to eliminate artifacts associated with microwave-frequency current flow within this electrode (between contact pads A and B) rather than through the tunnel junction. The bias dependence of the differential resistance $\mathrm{d}V/\mathrm{d}I$ is shown in Fig. 1b for the parallel magnetization orientation (P, $\theta = 0°$, with θ the angle between $\hat{\mathbf{m}}$ and $\hat{\mathbf{M}}_{\mathrm{fixed}}$), antiparallel (AP, $\theta = 180°$) and intermediate angles. At zero bias, the tunnelling magnetoresistance

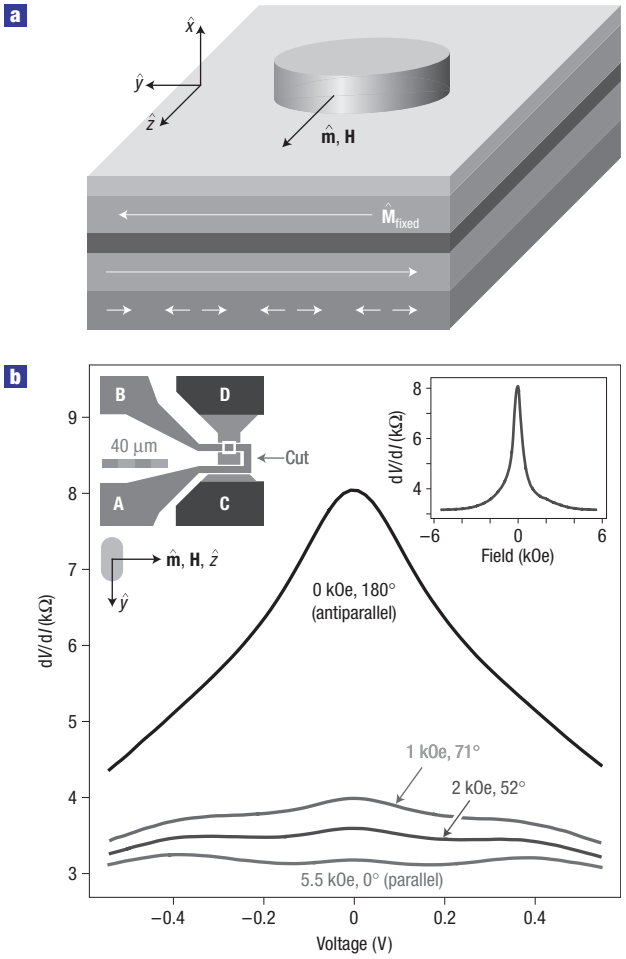

Figure 1 Magnetic tunnel junction geometry and magnetic characterization. **a**, Schematic diagram of the sample geometry. **b**, Bias dependence of differential resistance at room temperature for the parallel orientation of the magnetic electrodes ($\theta = 0^\circ$) and antiparallel orientation ($\theta = 180^\circ$), along with intermediate angles. The angles are determined assuming that the zero-bias conductance varies as cos(θ). Left inset: Layout of the electrical contacts (cropped), showing where the top electrode is cut to eliminate measurement artifacts. Right inset: Zero-bias magnetoresistance for H along $\hat{z}$.

ratio (TMR) is $[(dV/dI)_{AP} - (dV/dI)_P]/[(dV/dI)_P] = 154\%$. The TMR decreases to 43% at 540 mV bias, a fractional reduction of 72%. We estimate that the magnitude of the intrinsic critical current for spin-torque switching near $\theta = 0^\circ$ is $\geq 0.6 \pm 0.1$ mA ($\sim$1.8 V), on the basis of extrapolations to the nanosecond scale of pulsed-current switching measurements[20] made on samples from the same wafer. Our resonance measurements are made using biases much smaller than this.

The ST-FMR measurements[16,17] are made by first applying a sufficiently strong magnetic field H along the $\hat{z}$ direction (Fig. 1b inset) to saturate $\hat{\mathbf{m}}$, while $\hat{\mathbf{M}}_{fixed}$ is tilted to a lesser degree away from $\hat{y}$. We then bias the sample at room temperature with both a direct current I and a microwave-frequency current I_{RF} through a bias-tee, and sweep the frequency of I_{RF}. When spin-transfer from I_{RF} excites resonant magnetic dynamics, this causes the resistance to oscillate at the driving frequency. We measure the resonant d.c. voltage response, V_{mix}, that results from mixing between these resistance oscillations and I_{RF}. To maximize the signal-to-noise ratio of the measurement, we chop I_{RF} at 250 Hz and measure V_{mix} using a lock-in amplifier. In all cases, we use values of I_{RF} in the range 5–25 μA, small enough that the FMR response is in the linear regime.

Representative results for the ST-FMR spectra are shown in Fig. 2. We observe several magnetic resonances in the frequency range 2–14 GHz. Above 1.5 kOe, the spacing between the first two modes is 1.2–1.9 GHz in the three $50 \times 100\,nm^2$ devices we studied and 0.8–1.4 GHz in three $50 \times 150\,nm^2$ devices. The lowest-frequency resonance has by far the largest amplitude, and corresponds to the shape and sign of the signal expected for uniform excitation of the top magnetic layer[17]. We assume that other smaller resonances correspond to higher-frequency standing-wave modes of the top or bottom electrode, or perhaps coupled modes[17].

Our first major result is that the degree of asymmetry in the ST-FMR peak shape versus frequency for the lowest-frequency mode depends strongly on d.c. bias current I, with peak shapes for $I = 0$ being symmetric, and with the sign of the asymmetry depending on the sign of I (Fig. 2b). To analyse quantitatively the magnitudes and the peak shapes of the ST-FMR signals, we assume that the dynamics of the free magnetic layer near the main resonance peak can be described by a simple macrospin approximation, so that a generalized Landau–Lifshitz–Gilbert equation applies:

$$\frac{d\hat{\mathbf{m}}}{dt} = -\gamma\hat{\mathbf{m}} \times \mathbf{H}_{eff} + \alpha\hat{\mathbf{m}} \times \frac{d\hat{\mathbf{m}}}{dt} - \gamma\frac{\tau_\parallel(I,\theta)}{M_s\,\mathrm{Vol}}\hat{\mathbf{y}} - \gamma\frac{\tau_\perp(I,\theta)}{M_s\,\mathrm{Vol}}\hat{\mathbf{x}}. \quad (1)$$

Here γ is the magnitude of the gyromagnetic ratio, α is the Gilbert damping parameter, $\mathbf{H}_{eff}$ is an effective field as defined in ref. 21 and $M_s\,\mathrm{Vol} \approx (1.06 \pm 0.16) \times 10^{-14}$ e.m.u. is the total magnetic moment of the free layer on the basis of our estimate of the sample geometry and the measured value of $M_s = 1{,}100$ e.m.u. cm^{-3}, consistent with ref. 19. The resulting ST-FMR lineshapes have been evaluated[16,21,22], and good agreement has been observed in ST-FMR measurements on all-metal spin-valve devices[17]. By extending the analysis of ref. 21 to non-zero values of I (see Supplementary Information, Note 1), equation (1) predicts that the ST-FMR signal is to a good approximation

$$\langle V_{mix}\rangle = \frac{1}{4}\frac{\partial^2 V}{\partial I^2}I_{RF}^2 + \frac{1}{2}\frac{\partial^2 V}{\partial\theta\partial I}\frac{\hbar\gamma\sin\theta}{4eM_s\,\mathrm{Vol}\,\sigma} \times I_{RF}^2(\zeta_\parallel S(\omega) - \zeta_\perp\Omega_\perp A(\omega)). \quad (2)$$

Here $\zeta_\parallel = [(2e/\hbar)/\sin(\theta)]d\tau_\parallel/dI$ and $\zeta_\perp = [(2e/\hbar)/\sin(\theta)]\,d\tau_\perp/dI$ represent the differential torques in dimensionless units, $S(\omega) = 1/\{1+[(\omega-\omega_m)/\sigma]^2\}$ and $A(\omega) = [(\omega-\omega_m)/\sigma]S(\omega)$ are symmetric and antisymmetric lorentzians, σ is the linewidth, ω_m is the resonant precession frequency and $\Omega_\perp = \gamma(4\pi M_{eff} + H)/\omega_m$ for our geometry. We use $4\pi M_{eff} = 11 \pm 1$ kOe for the effective out-of-plane anisotropy, as determined from the magnetoresistance for H perpendicular to the substrate. The first term on the right in equation (2) is a non-resonant background, useful for calibrating I_{RF}. The second term gives the dominant ST-FMR signal; as a function of frequency it has the form of a symmetric lorentzian $\propto \zeta_\parallel \propto d\tau_\parallel/dI$, minus an antisymmetric lorentzian $\propto \zeta_\perp \propto d\tau_\perp/dI$.

As shown in Fig. 2b, the peak shapes for the ST-FMR signals of the lowest-frequency main resonance mode are fitted very well by the form expected from equation (2). From the fits, at each value of H and I we determine with high precision the

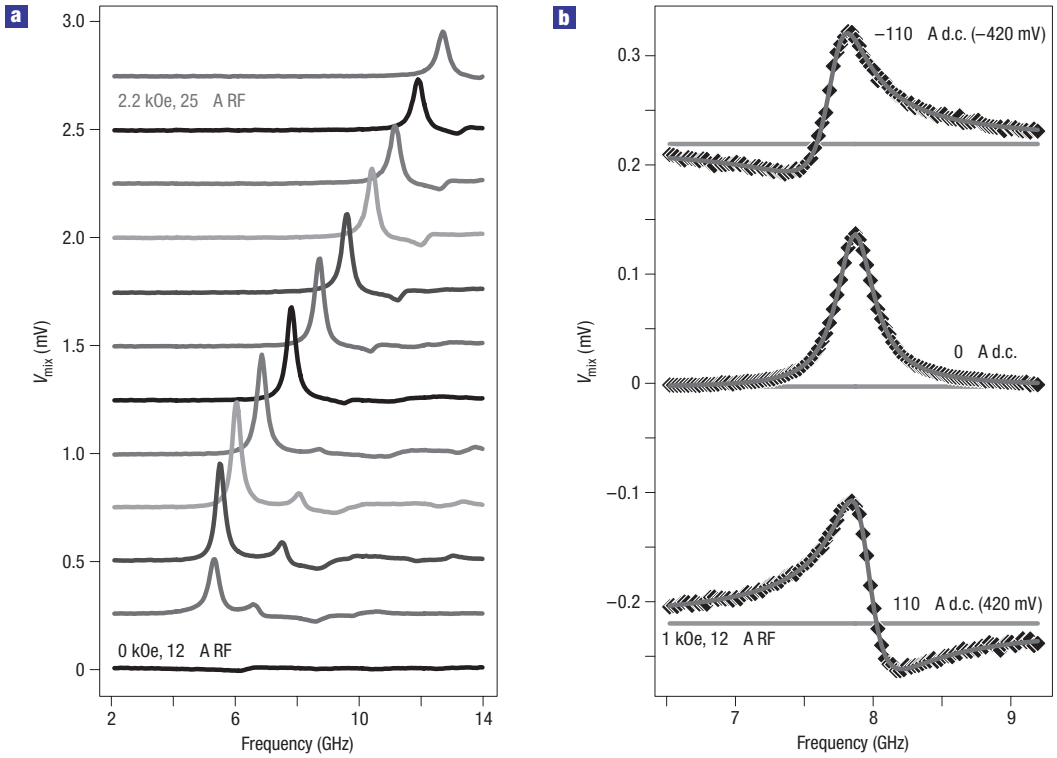

Figure 2 ST-FMR spectra at room temperature. a, Spin-transfer FMR spectra for $I = 0$, for magnetic fields (along $\hat{z}$) spaced by 0.2 kOe. I_{RF} ranges from 12 μA at low field (high resistance) to 25 μA at high field. The curves are offset by 250 μV. **b**, Details of the primary ST-FMR peaks at $H = 1{,}000$ Oe and $I_{RF} \approx 12$ μA for different d.c. biases. Symbols are data; lines are lorentzian fits. These curves are not artificially offset; the frequency-independent backgrounds for non-zero d.c. biases correspond to the first term on the right of equation (2). A d.c. bias also changes the degree of asymmetry in the peak shape versus frequency.

symmetric and antisymmetric peak amplitudes, the background, the linewidth σ and the resonant frequency ω_m. The raw results of these fits are shown in Supplementary Information, Fig. S1. To make a quantitative determination of $d\tau_\parallel/dI$ and $d\tau_\perp/dI$ using equation (2), it is necessary to calibrate the quantities I_{RF}^2 and $\partial^2 V/\partial\theta\partial I$, both of which depend on I owing to the bias dependence of the tunnel-junction impedance. We determine I_{RF}^2 from the non-resonant background signal, together with the value of $\partial^2 V/\partial I^2$ determined at low frequency. We calibrate $\partial^2 V/\partial\theta\partial I$ by measuring $\partial V/\partial I$ versus I at a sequence of magnetic fields in the $\hat{z}$ direction, assuming that the zero-bias conductance varies as $\cos(\theta)$ (and that θ depends negligibly on I), and then numerically differentiating $\partial V/\partial I$ with respect to θ at each value of I and H. These calibrations are sufficiently accurate that the uncertainty in our measurements is dominated by the uncertainty in the determination of M_sVol, not I_{RF} or $\partial^2 V/\partial\theta\partial I$ or the quality of fits to the peak shapes. Additional details concerning the calibration procedures are given in Supplementary Information, Note 2 and Figs S2,S3.

The most relevant final quantities for physical interpretation are expected to be the 'torkances'[18], $d\tau_\parallel/dV = (d\tau_\parallel/dI)/(dV/dI)$ and $d\tau_\perp/dV = (d\tau_\perp/dI)/(dV/dI)$. We plot these in Fig. 3a, as calculated from the measured values of dV/dI and the values of $d\tau_\parallel/dI$ and $d\tau_\perp/dI$ determined from the second term on the right-hand side of equation (2). ($d\tau_\parallel/dI$ and $d\tau_\perp/dI$ are plotted in Supplementary Information, Fig. S4 and the ratio $(d\tau_\perp/dV)/(d\tau_\parallel/dV)$ in Supplementary Information, Fig. S5.) We first consider the dependence of the torkances on θ. It is predicted[12–15,18] that for elastic tunnelling $d\boldsymbol{\tau}/dV$ should be proportional to $\sin(\theta)$. The inset to Fig. 3a shows that $(d\tau_\parallel/dV)/\sin(\theta)$ is indeed nearly constant over the range of angles measured, $45° < \theta < 90°$. Given this agreement, we divide out a factor of $\sin(\theta)$ in plotting the torkances in the main panel of Fig. 3a, so that the plotted results should be independent of angle. (θ is determined as discussed above.)

The bias dependence of the dominant, in-plane component of the torkance, $d\tau_\parallel/dV$, is shown in the main panel of Fig. 3a. At $V = 0$, we find $(d\tau_\parallel/dV)/\sin(\theta) = 0.13 \pm 0.02\hbar/(2e)\,\mathrm{k\Omega^{-1}}$. The value predicted[18] for elastic tunnelling in a symmetric junction of polarization P is

$$\frac{d\tau_\parallel/dV}{\sin\theta} = \frac{\hbar}{4e}\frac{2P}{1+P^2}\left(\frac{dI}{dV}\right)_P, \qquad (3)$$

which is equal to $0.144\hbar/(2e)\,\mathrm{k\Omega^{-1}}$ for $P = 0.66$ (corresponding to our TMR of 154%) and the value of parallel conductance $(dI/dV)_P = 1/(3.19\,\mathrm{k\Omega})$ for our device at $V = 0$. For $P = 1$, the prediction would be $0.157\hbar/(2e)\,\mathrm{k\Omega^{-1}}$. Therefore our measured torkance agrees with equation (3) to within experimental uncertainty, and is within 20% of the maximum value possible given our device conductance.

As a function of bias, we find that $d\tau_\parallel/dV$ is constant to within ±8% for $|V| \leq 300$ mV. This is in striking contrast to the magnetoresistance, which decreases by 50% over the same bias range (Fig. 1b). Furthermore, the value of $d\tau_\parallel/dV$ seems to increase for $300\,\mathrm{mV} < |V| < 540\,\mathrm{mV}$, whereas the magnetoresistance continues to decrease to just 28% of its full value. The low-bias result confirms with greater

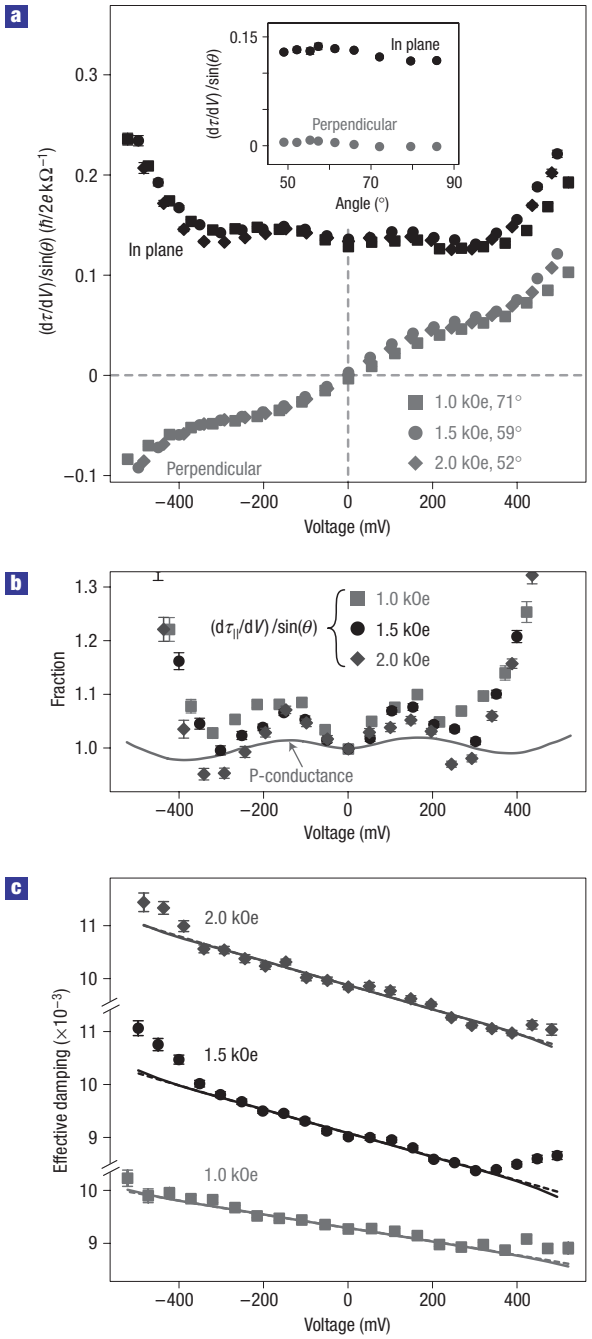

Figure 3 Bias dependence of the spin-transfer torkances and magnetic damping. a, Magnitudes of the in-plane and perpendicular torkance ($d\tau_\parallel/dV$ and $d\tau_\perp/dV$) determined from the room temperature ST-FMR signals, for three different values of applied magnetic field in the $\hat{z}$ direction. The overall scale for the torkances has an uncertainty of ~15% associated with the determination of the sample volume. Inset: Angular dependence of the torkances at zero bias. **b**, Comparison of the bias dependences of $d\tau_\parallel/dV$ and $(dI/dV)_P$, relative to their zero-bias values. Small background slopes (visible in **a**) are subtracted from the torkance values. **c**, Symbols: effective damping determined from the ST-FMR linewidths. Dashed lines: fits to equation (6) for $|V| < 300$ mV assuming $\partial\tau_\parallel/\partial V$ is independent of V. Solid lines: fits to equation (6) including the bias dependence of $\partial\tau_\parallel/\partial V$ shown in **b**.

sensitivity the conclusions in ref. 11, in which a combined effect of $\tau_\parallel/I$ and $\tau_\perp/I$ was measured for $|V| < 350$ mV in $Co_{90}Fe_{10}/MgO/Co_{90}Fe_{10}$ junctions.

The theoretical framework of ref. 18 provides a means to analyse these results. The differential conductances for parallel and antiparallel magnetic configurations and the in-plane spin-transfer torkance can all be written in terms of conductance amplitudes $G_{\sigma\sigma'}$ between spin channels ($\sigma, \sigma' = \pm$ are spin indices for the bottom and top electrodes). Assuming that the tunnelling mechanism itself does not depend on spin operators, we may write[13,18]

$$\frac{d\tau_\parallel}{dV} = \frac{\hbar}{4e}(G_{++} - G_{--} + G_{+-} - G_{-+})\sin(\theta) \qquad (4)$$

$$\left(\frac{dI}{dV}\right)_P = G_{++} + G_{--}, \qquad \left(\frac{dI}{dV}\right)_{AP} = G_{+-} + G_{-+}. \qquad (5)$$

The amplitudes $G_{\sigma\sigma'}$ can describe both elastic and inelastic tunnelling processes. With the assumptions that $G_{+-} \approx G_{-+}$ for a symmetric junction near zero bias and $G_{--} \ll G_{++}$, equations (4) and (5) imply that, approximately, $d\tau_\parallel/dV \propto (dI/dV)_P$. The observation that $d\tau_\parallel/dV$ is approximately independent of bias for $|V| < 300$ mV can therefore be related to the fact that the differential conductance for parallel moments is approximately independent of bias in this range as well. Figure 3b shows a direct comparison of the fractional changes in $d\tau_\parallel/dV$ and $(dI/dV)_P$ versus V. For $|V| < 300$ mV, $d\tau_\parallel/dV$ and $(dI/dV)_P$ show a similar pattern of non-monotonic variations, although the relative changes in $d\tau_\parallel/dV$ are greater. At larger biases, 300 mV $< |V| <$ 540 mV, the apparent experimental value of $d\tau_\parallel/dV$ increases much more rapidly than $(dI/dV)_P$. We suspect that much of this increase may be an artefact, rather than reflecting the true value of $d\tau_\parallel/dV$, because the values of $d\tau_\parallel/dV$ shown in Fig. 3a become larger than the maximum predicted for perfect spin polarization[13,18] and because in the same regime ($|V| > 300$ mV) the spin-torque model also fails to describe the resonance linewidths (see below). The upturn in the apparent value of $d\tau_\parallel/dV$ might conceivably be caused by hot-electron effects or heating[11,23], which are neglected in our model. If these effects decrease the total magnetic moment of the free layer (M_s Vol) at high bias, they could enhance the response of the magnet to a given torkance and artificially inflate our determination of $d\boldsymbol{\tau}/dV$.

Within the macrospin ST-FMR model (equation (2)), an antisymmetric-in-frequency component of the ST-FMR resonance can be related to an out-of-plane torkance, $d\tau_\perp/dV$. We observe only symmetric ST-FMR peaks at $V = 0$ (Fig. 2b), implying that at zero bias $d\tau_\perp/dV = 0$. This differs from a previous experimental report[16]. Figure 3a shows that the asymmetries we measure for $V \neq 0$ correspond to an approximately linear dependence of $d\tau_\perp/dV$ on V at low bias. This result is consistent with theoretical expectations[14] that for a symmetric tunnel junction the low-order bias dependence has the form $\tau_\perp(V)/\sin(\theta) = A_0 + A_1 V^2$ (with A_0 and A_1 independent of bias). For our full range of bias we measure $A_1 = (84 \pm 13)(\hbar/2e)\,G\Omega^{-1}\,V^{-1}$. The integrated torque $\tau_\perp(V)$ is in the $\hat{\mathbf{m}} \times \hat{\mathbf{M}}_{fixed}$ direction, and grows to be 30% of the in-plane torque $\tau_\parallel(V)$ at the largest bias we probe, in qualitative agreement with ref. 14. We do not believe that alternative mechanisms such as heating can account for the asymmetric peak shapes, as explained in Supplementary Information, Note 3.

We have also made ST-FMR measurements on metallic IrMn/Py/Cu/Py spin valves in the same experimental geometry, and in this case we find that the lowest-frequency peaks are frequency symmetric to within experimental accuracy for all biases $|I| < 2$ mA, from which we conclude that $\tau_\perp$ is always less than 1% of $\tau_\parallel$ (see Supplementary Information, Fig. S6). The ratio $\tau_\perp/\tau_\parallel < 1\%$ is much smaller than has been suggested for Co/Cu/Co metal spin valves on the basis of analysis of the dynamical phase diagram[24]. In our opinion it remains an open question

whether a significant perpendicular torkance can be generated in a current-perpendicular-to-the-plane all-metal spin valve.

The measured linewidths σ of our ST-FMR measurements on MgO junctions enable a determination of the magnetic damping. Assuming that $\tau_\parallel(V,\theta) \propto \sin(\theta)$, equation (1) implies (see Supplementary Information, Note 1),

$$\sigma = \frac{\alpha\omega_m}{2}(\Omega_\perp + \Omega_\perp^{-1}) - \cot(\theta)\frac{\gamma\tau_\parallel(V,\theta)}{2M_s\,\mathrm{Vol}}. \qquad (6)$$

In Fig. 3c we plot the bias dependence of the effective damping defined as $\alpha_{\mathrm{eff}} = 2\sigma/[\omega_m(\Omega_\perp + \Omega_\perp^{-1})]$. The zero-bias values give an average Gilbert damping coefficient $\alpha = 0.0095 \pm 0.0010$, consistent with literature reports for similar materials[25]. The dashed straight lines plotted in Fig. 3c show the slopes expected from equation (6), using as a fitting parameter that $(\partial\tau_\parallel/\partial V)/\sin(\theta) = (0.16 \pm 0.03)\,\mathrm{k}\Omega^{-1}\hbar/2e$ (assuming that $\partial\tau_\parallel/\partial V$ is constant as a function of V). This estimate agrees with the value determined independently above from the magnitude of the ST-FMR peaks near $V = 0$. Incorporating the apparent upturn of $\mathrm{d}\tau_\parallel/\mathrm{d}V$ at high bias into equation (6) produces little change in the predictions (solid lines in Fig. 3c). We find that the good agreement present at low bias between the measured linewidths and equation (6) breaks down for $|V| > 300$ mV, perhaps owing to ignoring heating or hot-electron effects as mentioned above.

Our measurements have several important implications. Our finding that the in-plane torkance $\partial\tau_\parallel/\partial V$ maintains its strength with increasing bias confirms that the spin-transfer torque can remain effective in magnetic-memory devices operated at high bias, despite the precipitous decrease of TMR with bias in such samples. We have found the magnitude of the in-plane torkance to be in quantitative agreement with the theoretical prediction of equation (3) for devices that have a tunnelling spin polarization $P = 0.66$. This formula predicts that for perfect polarization, $P = 1$, the in-plane torque should be only 8% stronger than for $P = 0.66$. From this we conclude that attempts to produce MTJs that have even higher tunnelling polarizations and TMR values are unlikely to improve the spin-torque-to-conductance ratio by more than this small amount, and efforts to improve MTJs for spin-torque applications should therefore focus on optimizing other properties, such as the total magnetic moment, damping, or magnetic anisotropy. The reason why the TMR and torkance are not more closely linked seems to be that inelastic tunnelling due to magnons[15], and generally other mechanisms not involving spin operators[18], may decrease TMR without affecting torkance in symmetric MTJs. Finally, we note that although we measure a significant perpendicular component of spin torque, this component has not previously been included in models of spin-torque-driven magnetic switching. Simulations with perpendicular torques induced by magnetic-field pulses suggest that a perpendicular spin-transfer torkance may alter the magnetic-moment trajectory during switching enough to assist efficient magnetic reversal[26], so this spin-torque component should be included in future modelling.

METHODS

DEVICE FABRICATION

The resistance–area product for parallel electrodes in our tunnel-junction multilayers is $\approx 12\ \Omega\,\mu\mathrm{m}^2$. The top $Co_{60}Fe_{20}B_{20}$ layer is patterned by electron-beam lithography and ion milling to produce a rectangular cross-section with rounded corners. The etch is stopped at the MgO barrier. Top contacts are made with 5 nm Ti/150 nm Cu/10 nm Pt. The contacts are originally fabricated in a four-probe arrangement as shown in Fig. 1b. However, we find that ST-FMR measurements in this geometry are affected by microwave-frequency current flowing within the patterned top electrode above the sample (rather than through the MgO tunnel barrier). This produces a significant microwave-frequency magnetic field with a phase different from the spin current, and changes the magnitude and the degree of asymmetry of the resonance peak. It also causes the FMR results to vary depending on which of the two top contacts (A or B in Fig. 1b) is used, whereas the results are the same on interchanging bottom contacts (C or D). To minimize this problem, we cut the top lead near the sample (see Fig. 1b), and then make the ST-FMR measurements using contacts B and D.

We use the convention that positive bias corresponds to electron flow down the pillar, giving a sign of $\tau_\parallel$ that favours antiparallel alignment of the top 'free' magnetic layer moment ($\hat{\mathbf{m}}$) relative to that of the lower layer ($\hat{\mathbf{M}}_{\mathrm{fixed}}$).

Received 22 May 2007; accepted 8 October 2007; published 25 November 2007.

References

1. Butler, W. H., Zhang, X. G., Schulthess, T. C. & MacLaren, J. M. Spin-dependent tunneling conductance of Fe|MgO|Fe sandwiches. *Phys. Rev. B* **63**, 054416 (2001).
2. Mathon, J. & and Umerski, A. Theory of tunneling magnetoresistance of an epitaxial Fe/MgO/Fe(001) junction. *Phys. Rev. B* **63**, 220403 (2001).
3. Parkin, S. S. P. *et al.* Giant tunnelling magnetoresistance at room temperature with MgO (100) tunnel barriers. *Nature Mater.* **3**, 862–867 (2004).
4. Yuasa, S., Fukushima, A., Suzuki, Y. & Ando, K. Giant room-temperature magnetoresistance in single-crystal Fe/MgO/Fe magnetic tunnel junctions. *Nature Mater.* **3**, 868–871 (2004).
5. Huai, Y., Albert, F., Nguyen, P., Pakala, M. & Valet, T. Observation of spin-transfer switching in deep submicron-sized and low-resistance magnetic tunnel junctions. *Appl. Phys. Lett.* **84**, 3118–3120 (2004).
6. Fuchs, G. D. *et al.* Spin-transfer effects in nanoscale magnetic tunnel junctions. *Appl. Phys. Lett.* **85**, 1205–1207 (2004).
7. Hosomi, M. *et al.* A novel nonvolatile memory with spin torque transfer magnetization switching: Spin-RAM. *IEDM Technical Digest, IEEE International* 459–462 (5–7 December 2005).
8. Kiselev, S. I. *et al.* Microwave oscillations of a nanomagnet driven by a spin-polarized current. *Nature* **425**, 380–383 (2003).
9. Kaka, S. *et al.* Mutual phase-locking of microwave spin torque nano-oscillators. *Nature* **437**, 389–392 (2005).
10. Mancoff, F. B., Rizzo, N. D., Engel, B. N. & Tehrani, S. Phase-locking in double-point-contact spin-transfer devices. *Nature* **437**, 393–395 (2005).
11. Fuchs, G. D. *et al.* Spin torque, tunnel-current spin polarization, and magnetoresistance in MgO magnetic tunnel junctions. *Phys. Rev. Lett.* **96**, 186603 (2006).
12. Slonczewski, J. C. Conductance and exchange coupling of two ferromagnets separated by a tunneling barrier. *Phys. Rev. B* **39**, 6995–7002 (1989).
13. Slonczewski, J. C. Currents, torques, and polarization factors in magnetic tunnel junctions. *Phys. Rev. B* **71**, 024411 (2005).
14. Theodonis, I., Kioussis, N., Kalitsov, A., Chshiev, M. & Butler, W. H. Anomalous bias dependence of spin torque in magnetic tunnel junctions. *Phys. Rev. Lett.* **97**, 237205 (2006).
15. Levy, P. M. & Fert, A. Spin transfer in magnetic tunnel junctions with hot electrons. *Phys. Rev. Lett.* **97**, 097205 (2006).
16. Tulapurkar, A. A. *et al.* Spin-torque diode effect in magnetic tunnel junctions. *Nature* **438**, 339–342 (2005).
17. Sankey, J. C. *et al.* Spin-transfer-driven ferromagnetic resonance of individual nanomagnets. *Phys. Rev. Lett.* **96**, 227601 (2006).
18. Slonczewski, J. C. & Sun, J. Z. Theory of voltage-driven current and torque in magnetic tunnel junctions. *J. Magn. Magn. Mater.* **310**, 169–175 (2007).
19. Kubota, H. *et al.* Dependence of spin-transfer switching current on free layer thickness in Co–Fe–B/MgO/Co–Fe–B magnetic tunnel junctions. *Appl. Phys. Lett.* **89**, 032505 (2006).
20. Yagami, K., Tulapurkar, A. A., Fukushima, A. & Suzuki, Y. Inspection of intrinsic critical currents for spin-transfer magnetization switching. *IEEE Trans. Magn.* **41**, 2615–2617 (2005).
21. Kovalev, A. A., Bauer, G. E. W. & Brataas, A. Current-driven ferromagnetic resonance, mechanical torques, and rotary motion in magnetic nanostructures. *Phys. Rev. B* **75**, 014430 (2007).
22. Kupferschmidt, J. N., Adam, S. & Brouwer, P. W. Theory of the spin-torque-driven ferromagnetic resonance in a ferromagnet/normal-metal/ferromagnet structure. *Phys. Rev. B* **74**, 134416 (2006).
23. Fuchs, G. D. *et al.* Adjustable spin torque in magnetic tunnel junctions with two fixed layers. *Appl. Phys. Lett.* **86**, 152509 (2005).
24. Zimmler, M. *et al.* Current-induced effective magnetic fields in Co/Cu/Co nanopillars. *Phys. Rev. B* **70**, 184438 (2004).
25. Bilzer, C. *et al.* Study of the dynamic magnetic properties of soft CoFeB films. *J. Appl. Phys.* **100**, 053903 (2006).
26. Ito, K., Devolder, T., Chappert, C., Carey, M. J. & Katine, J. A. Micromagnetic simulation of spin transfer torque switching combined with precessional motion from a hard axis magnetic field. *Appl. Phys. Lett.* **89**, 252509 (2006).

Acknowledgements

We thank Y. Nagamine, D. D. Djayaprawira, N. Watanabe and K. Tsunekawa of Canon ANELVA Corp. for providing the junction thin-film stack we used to fabricate the tunnel-junction devices in this study, and G. D. Fuchs and K. V. Thadani for discussions. J.Z.S. would like to acknowledge discussions with S. Assefa, W. J. Gallagher on sample processing techniques, X. Jiang and S. S. P. Parkin for sample fabrication assistance, M. Rooks and N. Ruiz for e-beam lithography support and the support of the IBM MRAM team as a whole. Cornell acknowledges support from the Office of Naval Research, from the NSF (DMR-0605742) and from the NSF/NSEC program through the Cornell Center for Nanoscale Systems. We also acknowledge NSF support through use of the Cornell Nanofabrication Facility/NNIN and the Cornell Center for Materials Research facilities.

Correspondence and requests for materials should be addressed to D.C.R.

Supplementary Information accompanies this paper on www.nature.com/naturephysics.

Author contributions

The first author played the primary role in making the measurements and analysing the data. J.Z.S. led the sample fabrication. Y.T.C. and J.Z.S. assisted in making measurements. All of the authors contributed to the data analysis and the preparation of the manuscript.